

Article

Microstructure and Properties of Monolayer Ta and Multilayer Ta/Ti/Zr/Ta Coatings Deposited on Biomedical Ti-6Al-4V Alloy by Magnetron Sputtering

Suli Zhao ^{1,3,†}, Shuguang Liu ^{2,*,†} , Yongjie Xue ², Ning Li ¹, Kuixue Xu ¹, Weiwei Qiu ², Xuexian Li ², Jinbo Wang ¹, Qian Wu ¹ and Chunbao Shi ¹

¹ Beijing Chunlizhengda Medical Instruments Co., Ltd., Beijing 101112, China; zhaosuli@clzd.com (S.Z.)

² Engineering Research Center for Electrophysical Apparatus and Application Technology, Beijing Research Institute of Automation for Machinery Industry Co., Ltd., Beijing 100120, China

³ Medical School of Nanjing University, Nanjing University, Nanjing 210093, China

* Correspondence: liushg@riamb.ac.cn

† These authors contributed equally to this work.

Abstract: Two types of coatings, i.e., monolayer Ta and multilayer Ta/Ti/Zr/Ta coatings, were deposited on biomedical Ti6Al4V (TC4) alloy by magnetron sputtering to improve its performance. To evaluate the effect of the two coatings on the alloy properties, the microstructure, composition, mechanical and tribological properties, in vitro biocompatibility, and corrosion resistance were investigated. The results showed that α -Ta exists in the monolayer Ta coating, while α -Ta and β -Ta phases coexist in the multilayer Ta/Ti/Zr/Ta coating. The multilayer Ta/Ti/Zr/Ta coating possessed the highest hardness and the monolayer Ta coating had the lowest friction coefficient compared to the Ti6Al4V alloy. The friction and wear tests revealed that the anti-wear performance of the Ta coating is the best, followed by that of the Ta/Ti/Zr/Ta coating, while the anti-wear performance of TC4 alloy is relatively poor in comparison with the Ta and Ta/Ti/Zr/Ta coatings. The wear resistance of the multilayer Ta/Ti/Zr/Ta coating under low normal load is better than that under high load normal load. Finally, the in vitro and electrochemical corrosion tests showed that the Ta coating modification provides better biocompatibility and corrosion resistance than those of the uncoated Ti6Al4V alloy.

Keywords: titanium alloy; coating; wear; biocompatibility; corrosion resistance



Citation: Zhao, S.; Liu, S.; Xue, Y.; Li, N.; Xu, K.; Qiu, W.; Li, X.; Wang, J.; Wu, Q.; Shi, C. Microstructure and Properties of Monolayer Ta and Multilayer Ta/Ti/Zr/Ta Coatings Deposited on Biomedical Ti-6Al-4V Alloy by Magnetron Sputtering. *Coatings* **2023**, *13*, 1234. <https://doi.org/10.3390/coatings13071234>

Academic Editor: Anita Ioana Visan

Received: 9 June 2023

Revised: 6 July 2023

Accepted: 7 July 2023

Published: 11 July 2023



Copyright: © 2023 by the authors. Licensee MDPI, Basel, Switzerland. This article is an open access article distributed under the terms and conditions of the Creative Commons Attribution (CC BY) license (<https://creativecommons.org/licenses/by/4.0/>).

1. Introduction

Orthopedic biomaterials are used to repair or replace damaged bone tissue in humans, aiming to reshape the anatomical structure and restore the original function [1]. An ideal orthopedic biomaterial should not only possess excellent mechanical and corrosion resistance properties, but also exhibit good biocompatibility and bioactivity [2,3]. Medical grade titanium (Ti) and its alloys are commonly used in bone biomaterials. Although several novel Ti alloys are emerging, the Ti6Al4V alloy is the most widely (such as hip joints, dental implants, prostheses, etc.) due to its superior performance in terms of relatively low elastic modulus, good biocompatibility, and suitable mechanical support [4–8]. Nevertheless, there are certain disadvantages when it is in contact with body fluids, such as the release of biotoxic metal ions (e.g., V^{5+} and Al^{3+}); Moreover, its relatively poor wear resistance restricts the application in organisms and thus, its application has been limited [9–11]. Hence, further advancements in the surface properties of the Ti6Al4V alloy in terms of high wear resistance, good corrosion resistance, and biocompatibility are still necessary.

Modification of the Ti6Al4V alloy surface is an important method used to effectively improve its surface properties [12,13]. Tantalum (Ta) has high hardness, excellent wear resistance, biocompatibility, as well as other important biological properties [12]. Moreover, Ta can provide better performance as regards corrosion resistance and biological activity

compared to Ti alloys. Therefore, more attention has recently been paid to Ta as a biomaterial [14–17]. However, Ta is a rare metal with very little reserves and of an extremely expensive price, which all significantly limit its application [18]. Previous studies have shown that the properties of a dense Ta coating with a substantial thickness are comparable to those of Ta metal [19,20]. Consequently, Ta coatings with a certain thickness have become a hot topic as an alternative. Ta coatings can be deposited on Ti alloys by thermal spraying (TS), chemical vapor deposition (CVD), and magnetron sputtering (MS) [21,22]. MS is considered an effective way to deposit a Ta coating, and coatings prepared by the MS method have many advantages, such as high quality, good completeness, and good controllability. Ta coatings comprise two crystalline phases, i.e., α -Ta phase with bcc structure and β -Ta phase with metastable tetragonal structure. In general, the β -Ta phase is harder and more brittle compared to the α -Ta phase [23,24].

Previous work showed that surface modification was used to enhance the mechanical and corrosion properties [25,26]. Certain research work has been conducted on the phase structure of Ta coatings to improve their performance. For example, Su et al. reported that the form of the α -Ta phase could be promoted at high pulsed bias; inversely, the form of the β -Ta phase could be promoted at low pulsed bias [27]. Colin et al. reported that there was no transition from β -Ta phase to α -Ta phase when the film thickness was increased or the deposited energy was altered [28]. The performance of Ta coatings prepared by MS is quite different. In addition, monolayer and multilayer Ta coatings have exhibited different performances [29]; The composite coating design method can improve the hardness and reduce the friction coefficient and adhesive wear [30]. However, the research studies on the surface properties of composite Ta have been rare. Therefore, it has become necessary to investigate the mechanical, corrosion, and biocompatibility properties of monolayer and multilayer Ta coatings prepared by MS, and determine the optimal performance.

In this work, monolayer Ta and multilayer Ta/Ti/Zr/Ta coatings were prepared on a biomedical grade Ti6Al4V ELI (TC4) alloy by MS. The microstructure and properties were characterized by X-ray diffraction (XRD), X-photoelectron spectroscopy (XPS), and scanning electron microscopy (SEM). The mechanical performance, tribological behavior, biocompatibility, and corrosion resistance were investigated by nano-indentation, friction, in vitro cytocompatibility, and electrochemical corrosion tests. The purpose of this work was to evaluate the effect of the monolayer Ta and multilayer Ta/Ti/Zr/Ta coatings on the TC4 alloy properties to provide a reference for the modification of TC4 alloy.

2. Materials and Methods

2.1. Substrate Preparation

The biomedical Ti6Al4V ELI alloy (ZhongNuo Advanced Material, Beijing, China), which strictly followed the GB/T 13810-2017 standard (first edition), served as the substrate. The substrate samples with dimensions of $\text{Ø}13 \text{ mm} \times 3 \text{ mm}$ were progressively ground by SiC sandpaper from 400# to 5000#, and then mechanically polished for 10 min with diamond pastes (Landnok Chemical, Guangzhou, China). Subsequently, the substrate samples were ultrasonically cleaned in 99.5% acetone and 99.5% alcohol (Macklin, Beijing, China) for 15 min respectively, and then blow-dried at room temperature. After that, their surface was sputter-cleaned by argon plasma in a vacuum chamber (Kurt J. Lesker PRO Line PVD, Kurt J. Lesker Company, Jefferson Hills, PA, USA) to remove any contamination.

2.2. Coating Deposition

Two types of Ta coatings were prepared: a monolayer Ta coating and a multilayer Ta/Ti/Zr/Ta coating. They were deposited on the above substrates using the MS system in pure argon gas. After the base vacuum of the system reached $2 \times 10^{-1} \text{ Pa}$, the substrate was heated up to $200 \text{ }^\circ\text{C}$. Pure Ta (99.95%, ZhongNuo Advanced Material, Beijing, China), Ti (99.995%, ZhongNuo Advanced Material, Beijing, China), and Zr (99.9%, ZhongNuo Advanced Material, Beijing, China) targets were driven by the sputtering power system, while the power was maintained at 150 W. All depositions were performed at a bias voltage

of -90 V. Prior to coating deposition, each target was cleaned by argon ion sputter-cleaning for 5 min. The monolayer Ta coating was deposited by the Ta target and the process lasted about 90 min. The Ti, Zr, and Ta layers were deposited alternately to obtain the multilayer coating. The deposition times for the Ti, Zr, and Ta targets during the multilayer coating deposition process were 90, 60, and 30 min, respectively.

2.3. Specimen Characterization

The phase compositions of the samples were examined by XRD analysis using a D/max-2500/PC diffractometer (DMAX-RB, Osaka, Japan). Their chemical bonding state was investigated by XPS (ESCALAB 250Xi, Waltham, MA, USA). Their morphology and thickness were observed by SEM (Hitachi SU5000, Tokyo, Japan). The nano-hardness and elastic modulus were determined through an in situ nanomechanical Triboindenter system (Billerica, MA, USA) under a maximum load of 5000 μ N, a loading rate of 500 μ N/s, and a dwelling time of 2 s. The tribological performance of the coating samples was assessed by the ball-disk reciprocating friction method with a load of 0.5 and 2 N at ambient atmosphere. SiC balls (\varnothing 6 mm) were utilized as the friction partner.

2.4. In Vitro Cytocompatibility Evaluation

Cell counting kit-8 (CCK-8, Merck, Rahway, NJ, USA) was adopted to evaluate the effect of the monolayer Ta and multilayer Ta/Ti/Zr/Ta coatings on the viability of MC3T3 pre-osteoblasts. After high-temperature and high-pressure steam sterilization, the samples were transferred to 24-well culture plates. Subsequently, 10% fetal bovine serum and 1% penicillin/streptomycin (Shanghai Yes Service Biotech, Shanghai, China) were added in the 24-well culture plates, which were then seeded with MC3T3 pre-osteoblast cells, and the extraction solution collected. Then, the control group was cultivated by complete medium, and the three treated groups were cultivated at a concentration of 25% extraction solution [31] in a humidified atmosphere (5% CO₂; 37 °C) for 24, 96, and 168 h, followed by phosphate buffered solution (PBS) washing (two times) to remove any unattached cells. After replacing the medium and cultivation at 37 °C for 4 h, the optical density (OD) of each well was determined according to the instructions of the manufacturer.

Furthermore, live and dead cell assay tests were conducted to further illustrate the coating cytotoxicity. The MC3T3 pre-osteoblasts cultivated for 24, 96, and 168 h with the sample were stained using a mixture of calcein-AM (4 mmol/L, Wuhan Chemstan Biotechnology, Wuhan, China) and propidium (2 mmol/L, Shanghai Honshun Biotechnology, Shanghai, China). After cultivation in the dark for 15–20 min, the cells were examined by fluorescence microscopy (MF52-N, Dongguan, China). The live cells appeared green in color and the dead cells appeared red.

2.5. Electrochemical Corrosion Tests

A potentiodynamic polarization technique was employed to assess the corrosion resistance of the uncoated TC4 and the monolayer Ta and multilayer Ta/Ti/Zr/Ta coatings. The potentiodynamic polarization measurements were conducted in simulated body fluid (SBF) solution [32] using a conventional three-electrode setup, where the sample functioned as the working electrode, a saturated calomel electrode was the reference electrode, and a Pt plate was utilized as the counter electrode. The tests were conducted within a potential range from -1.0 V vs. open circuit potential (OCP) to 2.0 V vs. OCP at a scanning rate of 1 mV/s.

3. Results and Discussion

3.1. Cross-Sectional Morphology

Figure 1a–c illustrates the schematic structure and macroscopic morphology of the uncoated TC4, monolayer Ta, and multilayer Ta/Ti/Zr/Ta coatings. It can be observed that the surface of all samples was smooth, while the monolayer and multilayer coatings appeared slightly yellow compared to the uncoated TC4 alloy. The TC4 alloy was composed

of α and β phase, with a near-equiaxed structure (Figure 1d). SEM images of the cross-sections of coating samples are exhibited in Figure 1e,f, where their thickness and structure can be observed. The Ta coating layer appeared relatively bright, while the Ti and Zr layers were dark. The thicknesses of the Ta and Ta/Ti/Zr/Ta coatings were about 3.28 and 3.10 μm , respectively (Figure 1b,c). Moreover, the thickness of each layer in the Ta/Ti/Zr/Ta coating was measured based on the coating structure and it was found to be 0.70 μm (first layer/Ta), 0.93 μm (second layer/Ti), 0.75 μm (third layer/Zr), and 0.72 μm (fourth layer/Ta). Moreover, it was observed that a columnar structure occurred in all coatings as in Figure 1e,f. In particular, the monolayer Ta coating in Figure 1e exhibited an apparent columnar structure perpendicular to the surface. In contrast, a less columnar structure was observed in the multilayer Ta/Ti/Zr/Ta coating. Su et al. [27] showed that the formation of the coarse columnar structures could be attributed to the longer deposition time of the monolayer Ta coating. The higher kinetic energy is considered to be responsible for the apparent columnar morphology observed in the monolayer Ta coating. Due to the longer sputtering time for the monolayer Ta coating preparation, more kinetic energy was accumulated, which caused an increase in the substrate temperature and led to a larger columnar structure. However, the large columnar structure was effectively inhibited during the multilayer coating preparation; that is, the growth of the continuous columnar structure was interrupted by inserting the Ta/Ti/Zr layers. In addition, except for being observed in each layer of the columnar structure, it could also be observed where the layers interface penetrated.

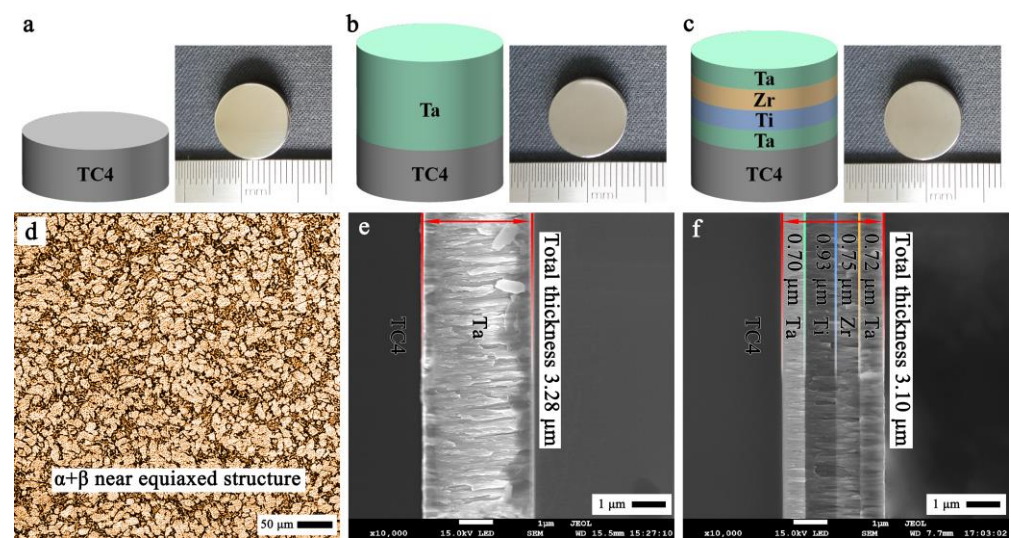


Figure 1. Schematics and macro-appearances of the (a) TC4 alloy, (b) Ta coating, and (c) Ta/Ti/Zr/Ta coating structure; (d) optical micrograph of the TC4 alloy; (e,f) cross-sectional SEM images of the Ta and Ta/Ti/Zr/Ta coatings, respectively.

3.2. Phase Characterization

Figure 2 depicts the XRD diagrams of the uncoated TC4, monolayer Ta, and multilayer Ta/Ti/Zr/Ta coatings. The diffraction peaks of the uncoated TC4 matched well with the peaks of the α -TC4 and β -TC4 phases. That is, the XRD patterns confirmed the existence of a dual-phase $\alpha + \beta$ microstructure in the uncoated TC4 substrate. As depicted in Figure 2, the monolayer Ta coating exhibited a simple pattern, and a main diffraction peak appeared, corresponding to the (110) face of α -Ta. Nevertheless, as regards the multilayer Ta/Ti/Zr/Ta coating, apart from the main diffraction peak, a relatively weak diffraction peak was found, with the two peaks corresponding to the (110) face of α -Ta and (002) face of β -Ta, respectively. Myers et al. [23] showed that the formation of the β -Ta phase can be attributed to the reduction of the coating thickness, and it is easier to form β -Ta phase in the thin-film Ta layer. Furthermore, no diffraction peak of the uncoated TC4 was

detected in both the monolayer and multilayer coatings, indicating that they covered the substrates entirely.

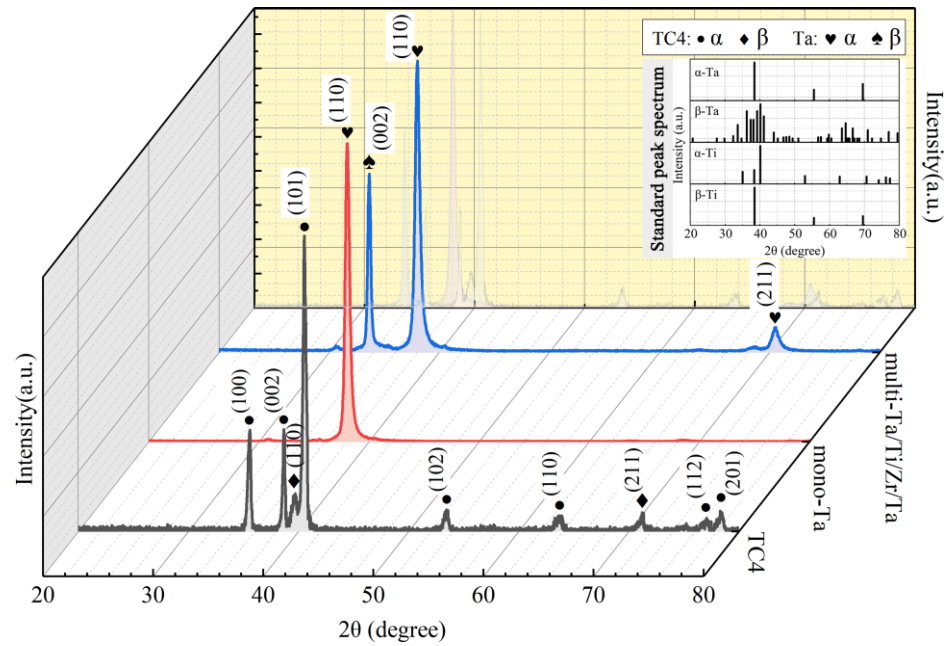


Figure 2. XRD patterns of the TC4 substrate and the two different Ta coatings.

Figure 3 presents the chemical states of the main elements in the uncoated TC4, monolayer Ta, and multilayer Ta/Ti/Zr/Ta coatings obtained by XPS. According to Figure 3a, the TC4 alloy surface contained Ti^{4+} elements, which indicates that the passive film of the TC4 alloy was primarily composed of TiO_2 . As can be observed in Figure 3b, the core-level spectrum of Ta 4f contained four groups of Ta peaks, and three chemical valence states of Ta existed. According to the literature [33], the peaks with a binding energy of 28.0 eV and 26.0 eV correlate to Ta_2O_5 , which are located at binding energies of 22.7 and 21.3 eV [27]. Colin et al. [28] reported that the presence of high valence oxides can stabilize the passivation film. Moreover, the main ingredients of the Ta coating also include TaO_2 and metallic Ta. In Figure 3c, it can be seen that the peak positions are identical with those in Figure 3b; that is, the main components of the multilayer coating surface were consistent with those of the monolayer coating surface.

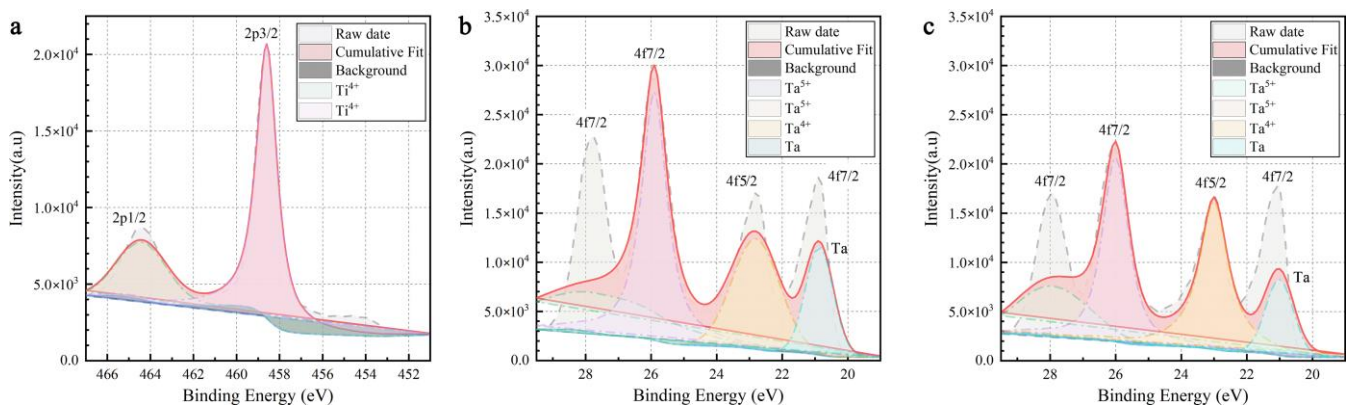


Figure 3. XPS spectra of the main components (Ti and Ta) in (a) the uncoated TC4, (b) monolayer Ta coating, and (c) multilayer Ta/Ti/Zr/Ta coating.

3.3. Mechanical Performance

The hardness (H) and elastic modulus (E) of the uncoated TC4, monolayer Ta, and multilayer Ta/Ti/Zr/Ta coatings were investigated by nano-indentation tests, and the corresponding results are presented in Figure 4. It can be observed that the load–depth curves are smooth, and the detection depth is less than 1/10 of the coating thickness, indicating that the effect of the substrate on the results was negligible. The maximum indentation and residual depths of the coated samples were both small compared to those of the uncoated TC4 sample, implying that the resistance to plastic deformation was enhanced after Ta coating deposition. In Figure 4b, it can be observed that both the nano-hardness and elastic modulus of the monolayer and multilayer Ta coatings are clearly higher than those of the uncoated TC4 substrate; that is, Ta coating deposition can improve the hardness of TC4 alloy. More specifically, the nano-hardness of the multilayer Ta/Ti/Zr/Ta coating was the highest, i.e., 10.3 GPa. This result reflects that the multilayer Ta/Ti/Zr/Ta coating performed better than the monolayer Ta one as regards the hardness of the TC4 substrate. In general, the hardness of the coatings is affected by the grain size, lattice type, and coating thickness. Combined with the above analysis, it can be deduced that the multilayer coating with alternately deposited layers can prevent the growth of the continuous columnar structure and efficiently refine the grain size. In addition, the sharp interlayer transitions could inhibit the motion of dislocations, which also is conducive to improving the hardness. Furthermore, previous studies have revealed that the typical hardness values of β -Ta are higher than those of α -Ta [23]. The above XRD results suggest that only α -Ta existed in the monolayer coating; on the contrary, one more phase of β -Ta existed in the multilayer coating, which is another important factor contributing to the higher micro-hardness of the multilayer coating.

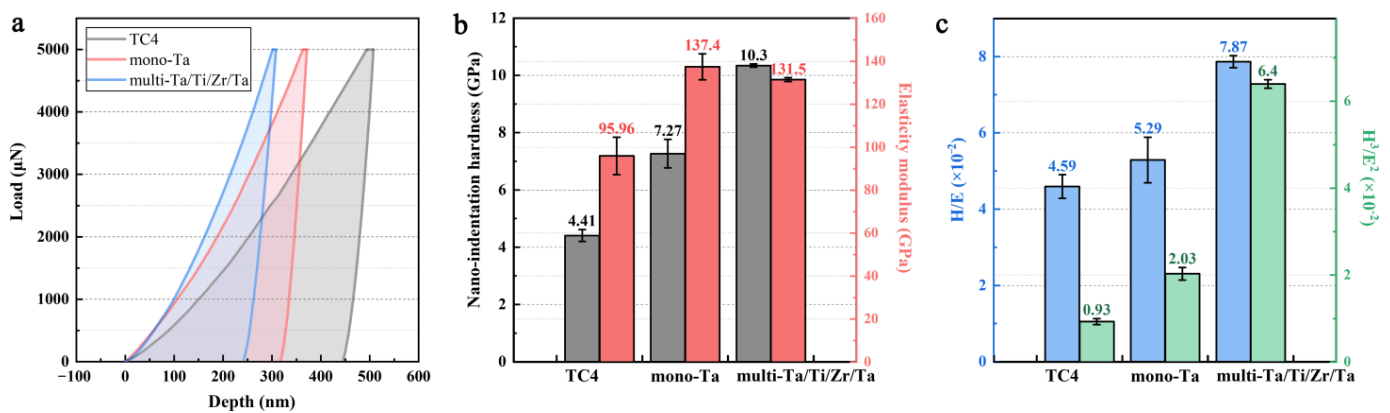


Figure 4. Nano-indentation results of uncoated and coated TC4 samples: (a) Load–depth curves; (b) E and H ; (c) H/E and H^3/E^2 .

Figure 4c presents the major parameters of H/E and H^3/E^2 obtained by calculation. The H/E is an important index for the wear resistance of coatings, while the H^3/E^2 can be used to evaluate the wear loss of coatings [34,35]. In general, the wear resistance of coatings with higher H/E and H^3/E^2 values is better than that of coatings with lower H/E and H^3/E^2 values. According to Figure 4c, the H/E and H^3/E^2 values of the multilayer Ta/Ti/Zr/Ta coating were the highest, suggesting that it might possess a better wear resistance.

3.4. Tribological Performance

Figure 5 shows the friction and wear curves of the uncoated TC4, monolayer Ta, and multilayer Ta/Ti/Zr/Ta coating samples sliding against SiC balls under normal loads of 0.5 and 2 N in an atmospheric environment, respectively. As can be observed, the friction coefficient curves of all samples are composed of two periods, i.e., the running-in and steady-wear periods; in all cases, the running-in periods were very short. During the running-in period, all friction coefficients increased with the elapsed friction time, which

can be attributed to the situation where the true contact area between the friction pairs increased rapidly, and the integrity of the sample surface was disrupted. Moreover, the friction coefficient curves of the samples tested under different conditions were quite different. Under a normal load of 0.5 N, the average friction coefficients of the uncoated TC4, monolayer Ta coating, and multilayer Ta/Ti/Zr/Ta coating were 0.618, 0.412, and 0.329, respectively. Apparently, the friction coefficient of the multilayer Ta/Ti/Zr/Ta coating was the lowest, under 0.5 N. Notably, both the curves of the monolayer Ta and multilayer Ta/Ti/Zr/Ta coatings presented two steady-wear periods (Figure 5a), which indicates that the wear of the friction pairs went through two different working environments. In the first steady-wear period, the friction coefficients were very small, since the coatings were undamaged during the early friction and wear stages; in contrast, in the second steady-wear period, the friction coefficients were relatively high. Under the normal load of 2 N (Figure 5b), all curves exhibited a longer running-in period compared to the corresponding curves obtained under 0.5 N. The average friction coefficients of the uncoated TC4, monolayer Ta coating, and multilayer Ta/Ti/Zr/Ta coating were 0.611, 0.529, and 0.564, respectively. This result shows that the friction coefficients of the two coatings were lower than that of the TC4 alloy, and that of the multilayer Ta/Ti/Zr/Ta coating was higher than that of the monolayer Ta coating, indicating the weaker adhesion strength of the multilayer coating under the higher normal load.

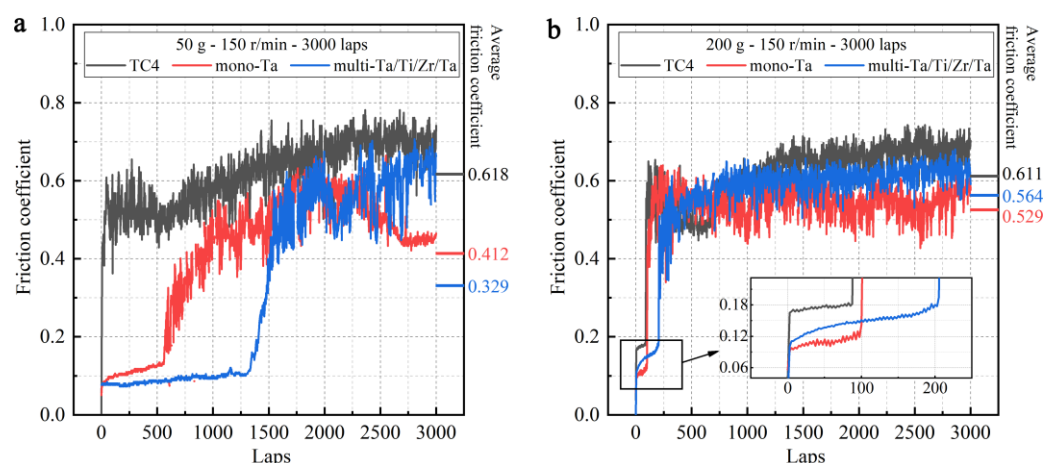


Figure 5. Friction coefficients of the uncoated TC4 and monolayer Ta and multilayer Ta/Ti/Zr/Ta coatings under normal loads of (a) 0.5 N and (b) 2 N.

Although the friction coefficient can quantify the lubrication effect of a material, it cannot directly reflect its wear resistance performance. To this end, the wear tracks were further investigated. Figure 6a–c. displays SEM and optical microscopy images of wear tracks on the uncoated and coated TC4 alloy samples sliding against SiC balls under a normal force of 0.5 N in an atmospheric environment. Obvious wear traces could be observed on the surface under 0.5 N normal load. More specifically, the uncoated TC4 alloy exhibited apparent parallel grooves with a considerable amount of adhered black debris. This was formed by micro-protrusions detached from the surface under the cutting action of the friction pair, indicating that the wear behavior of the uncoated TC4 was primarily adhesive wear. The corresponding 2D and 3D cross-sectional profiles are displayed in Figure 6(a3,a4), which demonstrate that the wear width and depth were 553.2 μm and 8.8 μm , respectively. Conversely, as depicted in Figure 6(b1–b4), the wear scar of the monolayer Ta coating was the slightest and with shallow grooves, and the corresponding 2D and 3D cross-section profiles in Figure 6(b3,b4) show that the wear track width and depth had minimum values of 409.6 μm and 1.9 μm , respectively. On the other hand, the multilayer Ta/Ti/Zr/Ta coating exhibited a relatively better wear resistance, with a wear width of 456.4 μm and depth of 5.6 μm , while a small amount of wear debris was

observed in the track. The wear width and depth of the three samples decreased in the order of TC4 > Ti/Zr/Ta > Ta. The wear rates of the uncoated and coated TC4 samples based on the wear track profiles are presented in Figure 6d. It can be observed that the uncoated TC4 alloy exhibited the highest wear rate ($2.16 \times 10^{-6} \text{ mm}^3/\text{N}\cdot\text{m}$), indicating that the wear resistance of the TC4 alloy was significantly enhanced after Ta coating modification. Among the coated samples, the monolayer Ta coating presented the lowest wear rate of $3.46 \times 10^{-7} \text{ mm}^3/\text{N}\cdot\text{m}$, which was about 30% lower than that of the multilayer Ta/Ti/Zr/Ta coating ($1.14 \times 10^{-6} \text{ mm}^3/\text{N}\cdot\text{m}$), and one order of magnitude lower than that of the TC4 alloy, suggesting an excellent anti-wear performance.

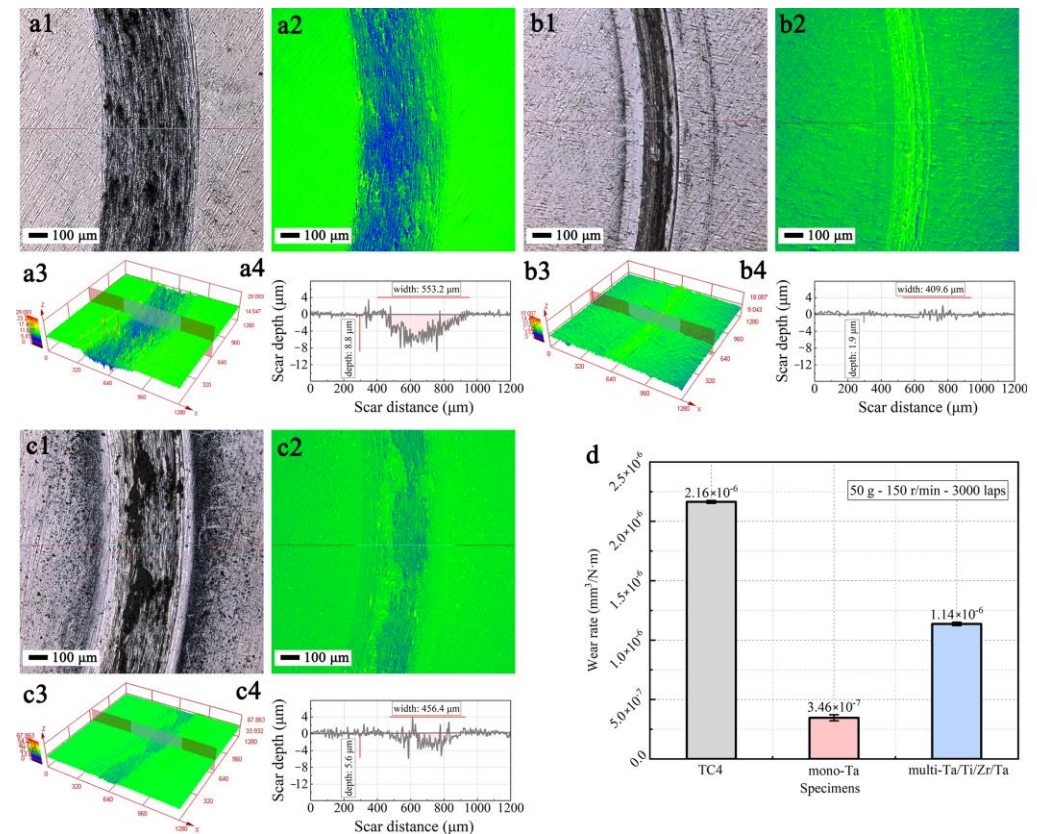


Figure 6. Wear tracks of the uncoated TC4 and the two coated samples under a normal load of 0.5 N. (a1–a4) TC4 alloy; (b1–b4) Ta coating; (c1–c4) Ta/Ti/Zr/Ta coating; (d) Wear rate of the different samples.

Figure 7a–c demonstrates the wear tracks along with the 2D and 3D morphologies of the uncoated and coated TC4 alloy samples sliding against SiC balls with a normal force of 2 N in an atmospheric environment. Under the normal load 2 N, the surface became severely worn compared to that of the corresponding samples tested under 0.5 N. Moreover, typical wide wear grooves and parallel furrows with a certain amount of wear debris occurred on all sample surfaces, indicating that the main wear mechanism was abrasive wear. The wear track data demonstrated that the Ta coating possessed the minimum width and depth values of 624.4 and 6.7 μm , respectively, and the uncoated TC4 presented the worst wear resistance. The corresponding values of the multilayer Ta/Ti/Zr/Ta coating were in the middle, i.e., width and depth of 629.8 μm and 10.0 μm , respectively. It is worth noting that the track depth on the Ta/Ti/Zr/Ta coating increased, which could be attributed to the weak adhesion strength of the coatings to the substrate under high normal load. This might have been caused by the poor adhesion of the multiple layers, and because each layer had a smaller thickness [36]. Moreover, Figure 7d presents the wear rate of the different samples based on the wear track profiles; the descending order of the wear rate

is as follows: TC4 > Ta/Ti/Zr/Ta > Ta. This agrees well with the result under the normal load of 0.5 N.

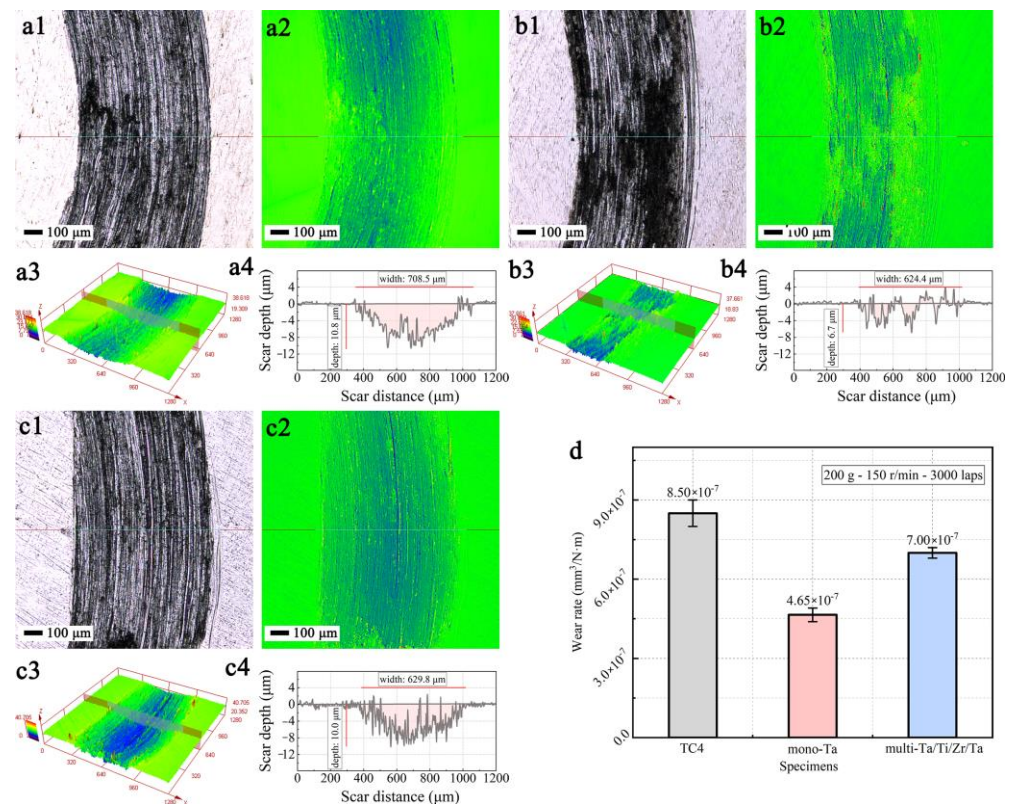


Figure 7. Wear tracks of the uncoated TC4 and the two coated samples under a normal load of 2 N. (a1–a4) TC4 alloy; (b1–b4) Ta coating; (c1–c4) Ta/Ti/Zr/Ta coating; (d) wear rate of the different samples.

To further investigate the wear behavior, Figure 8 shows high-magnification micrographs of the wear tracks on the uncoated and coated TC4 alloy samples sliding against SiC balls under normal loads of 0.5 and 2 N. Figure 8a–c demonstrates the typical worn surface morphologies obtained under a normal load of 0.5 N. As regards the TC4 alloy, a large amount of wear debris and a large adhesive area could be observed on the wear track (high-magnification image; rectangular region in Figure 8a), indicating that the wear mechanism involved adhesion wear. Since the harder friction pair wore down the TC4 alloy surface repeatedly, the detached debris produced a “cold welding” effect on the contact surface of the sample, forming adhesive nodes. Nevertheless, this bonding mode formed by “adhesion” is not strong. With the repeated trajectory movement of the friction pairs on the sample surface, the generated shear force continues to act on the trajectory of the wear track, driving some loosely bonded debris to form nodes and causing them to detach and transfer again, generating new accumulation nodes. As for the monolayer Ta coating under the normal load of 0.5 N, it can be observed that the coating fractured apparently after the wear experiment (Figure 8b). At higher magnification, it can be seen that the coating gradually peeled off, and there existed a cracked area, which was the main cause for the generation of abrasive particles. In contrast, the multilayer Ta/Ti/Zr/Ta coating was not worn away gradually, but a whole piece was worn away due to poor adhesion (Figure 8c). In addition, based on the higher magnification image, the edges of the coating were sharp, with a bright surface and cleavage plane. The presence of the coating could smooth the wear track morphology and reduce the wear adhesion zone.

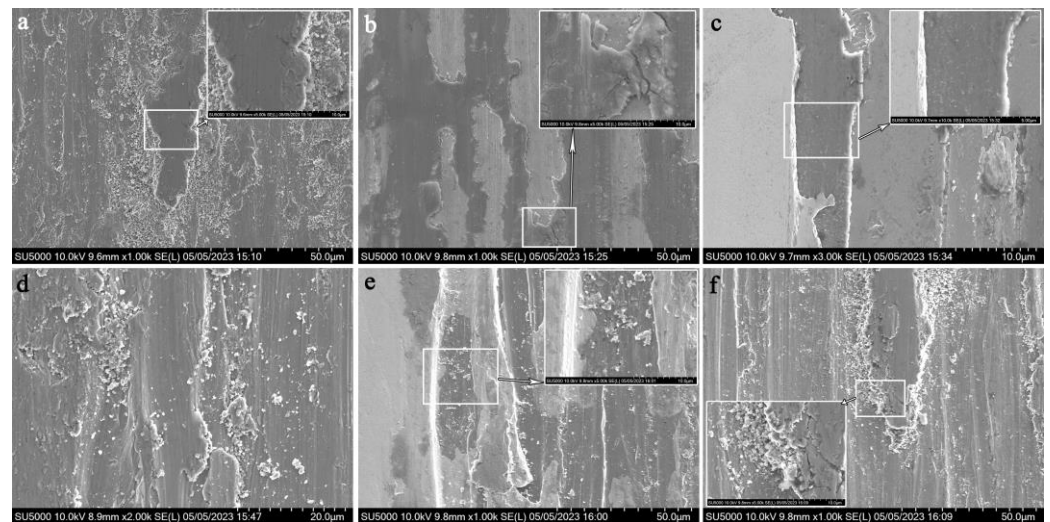


Figure 8. SEM images with magnified regions of the worn surfaces of (a) TC4 alloy under 0.5 N, (b) Ta coating under 0.5 N, (c) Ta/Ti/Zr/Ta coating under 0.5 N, (d) TC4 alloy under 2 N, (e) Ta coating under 2 N, and (f) Ta/Ti/Zr/Ta coating under 2 N.

Under the normal load of 2 N, the worn surface of the coated samples exhibited different characteristics from those under the normal load of 0.5 N. It can be observed that plastic deformation and multiple pear grooves parallel to the sliding direction of the friction pair appeared on the worn surface of the TC4 alloy (Figure 8d), indicating that the main wear mechanism was abrasive wear. Typical parallel grooves with black debris and plastic deformation morphology were observed on the worn surface of the Ta and Ta/Ti/Zr/Ta coatings, indicating abrasive wear (Figure 8e,f). In the magnification images of the typical morphologies, it can be seen that the phenomenon of debris accumulations occurred, especially in the multilayer Ta/Ti/Zr/Ta coating. This is due to that part of the coating being gradually peeled off which produces debris during the wear process, and the friction pair with increasing roughness scratch the surface, ultimately forming apparent grooves, corresponding to typical abrasive wear morphology. The coatings could protect the substrate and prevent wear over a certain period of time, reducing the overall plastic deformation of the alloy. Moreover, the Ta coating exhibited a better anti-wear performance than the Ta/Ti/Zr/Ta coating, which can be attributed to the poor adhesion of the multiple layers. On the other hand, the presence of β -Ta, which is harder than the α -Ta of the Ta/Ti/Zr/Ta coating, could promote brittle fracture.

3.5. *In Vitro* Cytocompatibility Evaluation

To illustrate the biocompatibility, the relative cell viability was tested to evaluate the cytotoxicity, and the results are depicted in Figure 9. As can be observed, the uncoated TC4 group had the lowest relative cell viability, and the number of cells decreased during incubation for 168 h. The monolayer and multilayer coating groups exhibited a higher relative cell viability than the uncoated TC4 group, which was close to that of the control group. Contrary to the uncoated TC4 group, the cell viability index of the Ta coating groups was significant increased by more than 10%, 30%, and 40% after incubation for 24 h, 96 h, and 168 h, respectively. To further evaluate the cytotoxicity of the coatings, live/dead staining was conducted to distinguish the live and dead cells. Figure 10 displays the fluorescence micrographs of live (green) and dead (red) cells on the control, uncoated TC4, monolayer Ta, and multilayer Ta/Ti/Zr/Ta coating groups after incubation for 24 h, 96 h, and 168 h. As shown in Figure 10, the cell morphology of the three experimental groups was similar to that of the control group. Almost every cell cultivated on the four groups was spindle-shaped and well-spread with lamellar extension and normal form. In addition, it was observed that, in each group, the cells proliferated with incubation time, and no

dead cells were found. Nevertheless, the cells in the uncoated TC4 group were relatively less than those in the other groups. After incubation for 24 and 96 h, the monolayer and multilayer coating groups possessed more cells than the control group. Notably, after 168 h, the number of cells in the multilayer coating group was relatively closer to that in the control group, while that in the monolayer group was lower than that in the control group. In addition, Li et al. [37] studied the cytotoxicity of metal Ta, and their results proved that the metal Ta exhibited excellent biocompatibility. This is consistent with our results. These results indicate that the Ta coating modification reduced the cytotoxicity of the TC4 alloy and improved its biocompatibility.

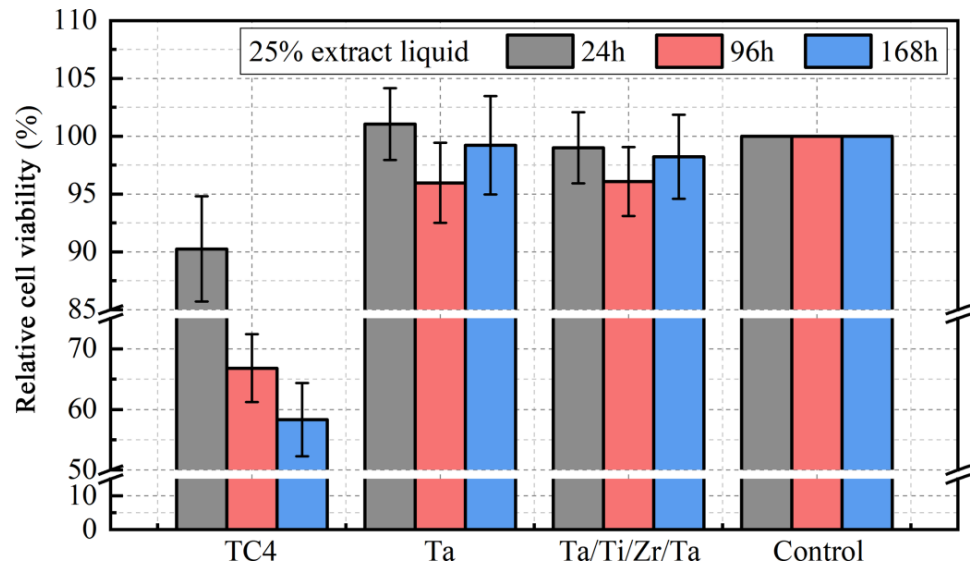


Figure 9. Relative cell viability of different samples after incubation for 24 h, 96, and 168 h.

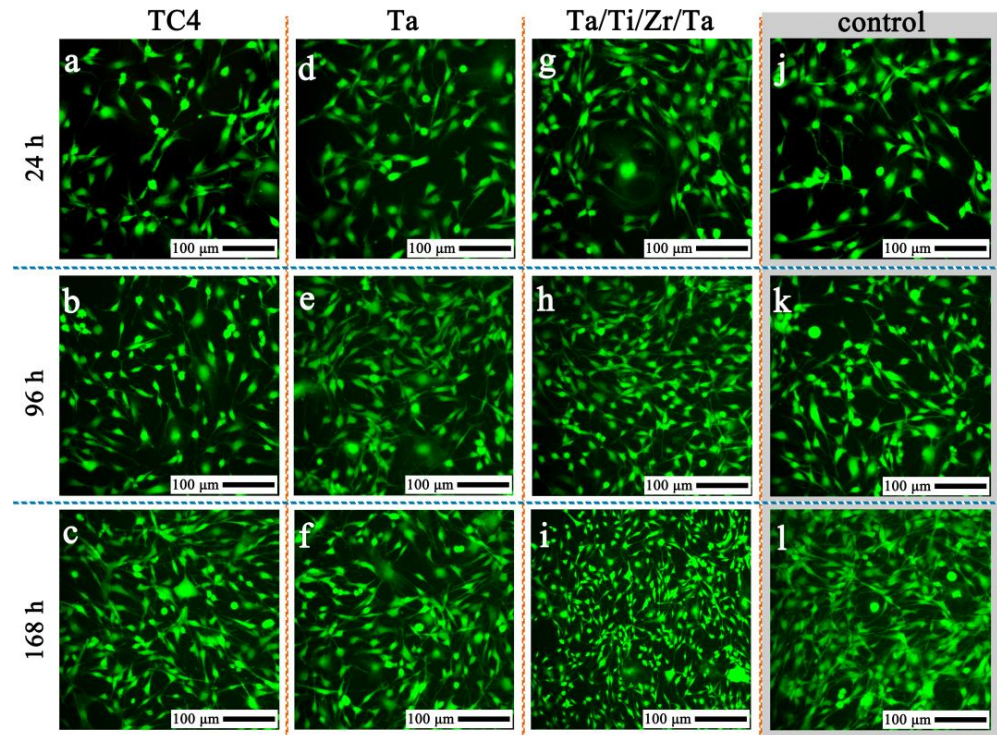


Figure 10. Fluorescence micrographs of live (green) and dead (red) cells on the different samples after incubation for (a,d,g,j) 24 h, (b,e,h,k) 96, and (c,f,i,l) 168 h.

3.6. Anti-Corrosion Properties

Corrosion resistance is another important index to evaluate the safety of implants. Therefore, the OCP-time and potentiodynamic polarization curves of the uncoated TC4, monolayer Ta, and multilayer Ta/Ti/Zr/Ta coating samples in SBF solution were obtained (Figure 11). According to Figure 11a, the OCP of the TC4 alloy shifted towards a lower value with increasing immersion time. Inversely, the OCP of the monolayer Ta and multilayer Ta/Ti/Zr/Ta coatings shifted towards a higher value with increasing time. This indicates that the passivation film on the surface of the TC4 alloy dissolved gradually with increasing immersion time, while the Ta and Ta/Ti/Zr/Ta coatings were stable and effective. The relevant electrochemical parameters, including the corrosion potential (E_{corr}), corrosion current density (I_{corr}), and passivation current density (I_p) obtained by the Tafel curve extrapolation method are listed in Table 1. The results suggest that the I_{corr} of both coating samples was lower than that of the uncoated TC4. In addition, the corrosion behavior of the uncoated TC4 and the two coated samples were clearly different. According to the polarization curves (Figure 11b), when the potential reached about 0.20 V, activation characteristics still existed in the anodic polarization curve of the uncoated TC4 alloy. In contrast, as regards the monolayer Ta sample, a long and stable passivation district was observed near the potential of 0.19 V. Notably, the polarization curve of the multilayer Ta/Ti/Zr/Ta coating exhibited a similar trend with the monolayer Ta coating. In general, the low I_{corr} and stable passivation zone suggest that the anti-corrosion performance of the two coatings was excellent compared to that of the uncoated TC4. This improvement in the corrosion resistance can be attributed to the change in the passivation film composition after Ta modification. Previous research reported that the presence of high valence oxides can stabilize the passivation film and reduce the corrosion rate [38]. Combined with the above XPS analysis results, it can be deduced that the major components in the surface of the monolayer and multilayer coatings were Ta_2O_5 and TaO_2 ; therefore, both the Ta and Ta/Ti/Zr/Ta coatings possessed better corrosion resistance.

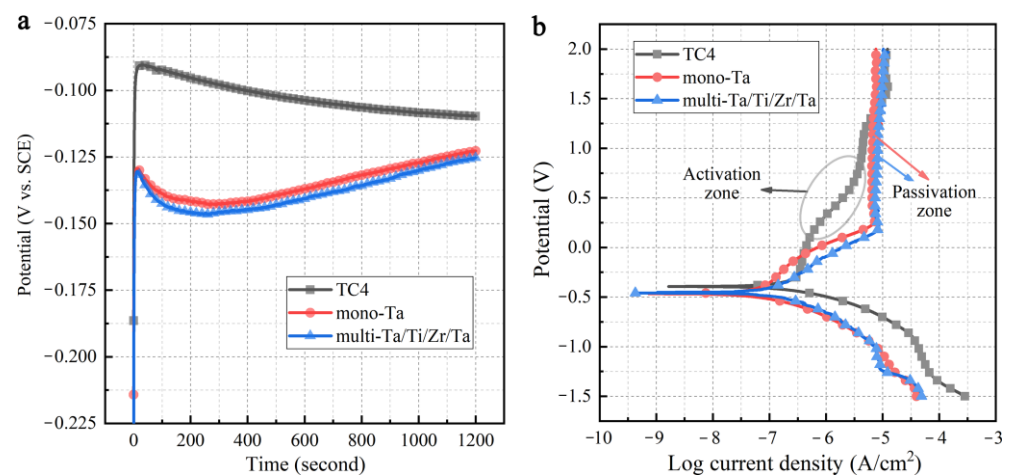


Figure 11. (a) OCP-time, and (b) potentiodynamic polarization curves of the uncoated TC4, monolayer, and multilayer coatings in SBF.

Table 1. Electrochemical corrosion parameters of the TC4 alloy with and without coatings.

Sample	I_{corr} (A/cm^2)	E_{corr} (V)
TC4 alloy	2.974×10^{-7}	-0.350
Mono-Ta	0.994×10^{-7}	-0.412
Multi-Ta/Ti/Zr/Ta	1.093×10^{-7}	-0.428

4. Conclusions

In this study, monolayer Ta and multilayer Ta/Ti/Zr/Ta coatings were deposited on the surface of biomedical Ti6Al4V by MS. Their structure and basic properties were investigated, and the main conclusions can be drawn as follows:

- (1) The monolayer Ta coating was composed of α -Ta phase and exhibited an apparent columnar structure due to the higher kinetic energy caused by the longer sputtering time. In contrast, the multilayer Ta/Ti/Zr/Ta coating consisted of α -Ta and β -Ta phases, and the columnar structure was effectively suppressed. Moreover, the principal compositions of the two coatings were consistent, including Ta₂O₅, TaO₂, and metallic Ta.
- (2) In comparison to the uncoated TC4 alloy, the surface hardness of both the Ta and Ta/Ti/Zr/Ta coatings was improved, with that of the Ta/Ti/Zr/Ta coating being higher than that of the Ta coating. This can be attributed to the suppression of the columnar structure and the presence of the β -Ta phase. The friction and wear tests revealed that the friction coefficient of the TC4 alloy was decreased after depositing the monolayer or multilayer coatings, and the anti-friction effect of the multilayer Ta/Ti/Zr/Ta under 0.5 N was better than that under 2 N due to the poor adhesion under high normal load. Overall, the order of the wear resistance regardless of the load magnitude was Ta > Ta/Ti/Zr/Ta > TC4.
- (3) The cell viability index was significantly improved, and the cytotoxicity was low after the coating modification. The electrochemical tests demonstrated that both the monolayer and multilayer coating modification could provide excellent corrosion resistance to the TC4 alloy. This study can thus provide a feasible way to improve the performance of Ta coatings on TC4 alloys.

The results show that the multilayer Ta/Ti/Zr/Ta coating will face the risk of weak layer-substrate and layer-layer adhesion in practical application, and the possibility of coating failure is greater. Compared to multilayer Ta/Ti/Zr/Ta coating, the monolayer Ta coating possessed better surface hardness and tribological properties, because its structure type and phase composition were easier to control. Moreover, the monolayer Ta coating had a certain wear reduction effect. In summary, the monolayer Ta coating is beneficial for preventing the precipitation of harmful elements such as Al and V in the substrate, reducing the risk of TC4 substrate wear and has greater application potential. In future work, we will continue to conduct research on multilayer coatings, and are committed to solving the problem of insufficient adhesion strength in multilayer coating. We hope to develop high-performance coating technology with better surface properties and more conducive to human implantation, providing theoretical support and expanding new ideas for the research and development of orthopedic implant products.

Author Contributions: Methodology, writing and editing, S.Z.; conceptualization and supervision, S.L.; software and validation, Y.X.; formal analysis, N.L.; project administration, K.X.; visualization and review, W.Q.; data curation, X.L.; investigation, J.W. and Q.W.; resources, C.S. All authors have read and agreed to the published version of the manuscript.

Funding: This work was supported by Beijing Postdoctoral Research Foundation (Grant Nos. 2022-ZZ-057 and 2021-ZZ-075).

Institutional Review Board Statement: Not applicable.

Informed Consent Statement: Not applicable.

Data Availability Statement: The raw/processed data required to reproduce these findings cannot be shared at this time as the data also form part of an ongoing study.

Conflicts of Interest: The authors declare no conflict of interest.

References

1. Yu, X.; Tang, X.; Gohil, S.V.; Laurencin, C.T. Biomaterials for Bone Regenerative Engineering. *Adv. Healthc. Mater.* **2015**, *4*, 1268–1285. [[CrossRef](#)]
2. Pham, V.-H.; Lee, S.-H.; Li, Y.; Kim, H.-E.; Shin, K.-H.; Koh, Y.-H. Utility of tantalum (Ta) coating to improve surface hardness in vitro bioactivity and biocompatibility of Co–Cr. *Thin Solid Films* **2013**, *536*, 269–274. [[CrossRef](#)]
3. Bartolomeu, F.; Dourado, N.; Pereira, F.; Alves, N.; Miranda, G.; Silva, F.S. Additive manufactured porous biomaterials targeting orthopedic implants: A suitable combination of mechanical, physical and topological properties. *Mater. Sci. Eng. C* **2020**, *107*, 110342. [[CrossRef](#)] [[PubMed](#)]
4. Atar, E.; Kayali, E.S.; Cimenoglu, H. Characteristics and wear performance of borided Ti6Al4V alloy. *Surf. Coat. Technol.* **2008**, *202*, 4583–4590. [[CrossRef](#)]
5. Komotori, J.; Lee, B.J.; Dong, H.; Dearnley, P.A. Corrosion response of surface engineered titanium alloys damaged by prior abrasion. *Wear* **2001**, *251*, 1239–1249. [[CrossRef](#)]
6. Rack, H.J.; Qazi, J.I. Titanium alloys for biomedical applications. *Mater. Sci. Eng. C* **2006**, *26*, 1269–1277. [[CrossRef](#)]
7. Deng, H.; Xu, K.; Liu, S.; Zhang, C.; Zhu, X.; Zhou, H.; Xia, C.; Shi, C. Impact of Engineering Surface Treatment on Surface Properties of Biomedical TC4 Alloys under a Simulated Human Environment. *Coatings* **2022**, *12*, 157. [[CrossRef](#)]
8. Zhao, S.; Liu, S.; Liu, Y.; Liu, X.; Xu, K.; Shi, C.; Jiang, Q. Influence of Zr content on immersion and electrochemical corrosion behavior of as-cast TiZr alloys. *Anti-Corros. Methods Mater.* **2022**, *69*, 603–610. [[CrossRef](#)]
9. Raj, V.; Mumjitha, M.S. Fabrication of biopolymers reinforced TNT/HA coatings on Ti: Evaluation of its Corrosion resistance and Biocompatibility. *Electrochim. Acta* **2015**, *153*, 1–11. [[CrossRef](#)]
10. Ding, Z.; Tang, Y.; Liu, L.; Ding, Z.; Tan, Y.; He, Q. Improving the adhesive, mechanical, tribological properties and corrosion resistance of reactive sputtered tantalum oxide coating on Ti6Al4V alloy via introducing multiple interlayers. *Ceram. Int.* **2022**, *48*, 5983–5994. [[CrossRef](#)]
11. Okazaki, Y.; Gotoh, E. Comparison of metal release from various metallic biomaterials In Vitro. *Biomaterials* **2005**, *26*, 11–21. [[CrossRef](#)]
12. Lin, W.T.; Lin, Z.W.; Kuo, T.Y.; Chien, C.S.; Huang, J.W.; Chung, Y.L.; Chang, C.P.; Ibrahim, M.Z.; Lee, H.T. Mechanical and biological properties of atmospheric plasma-sprayed carbon nanotube-reinforced tantalum pentoxide composite coatings on Ti6Al4V alloy. *Surf. Coat. Technol.* **2022**, *437*, 128356. [[CrossRef](#)]
13. Ding, Z.; Zhou, Q.; Wang, Y.; Ding, Z.; Tang, Y.; He, Q. Microstructure and properties of monolayer, bilayer and multilayer Ta₂O₅-based coatings on biomedical Ti-6Al-4V alloy by magnetron sputtering. *Ceram. Int.* **2021**, *47*, 1133–1144. [[CrossRef](#)]
14. Rahmati, B.; Sarhan, A.A.D.; Zalnezhad, E.; Kamiab, Z.; Dabbagh, A.; Choudhury, D.; Abas, W.A.B.W. Development of tantalum oxide (Ta-O) thin film coating on biomedical Ti-6Al-4V alloy to enhance mechanical properties and biocompatibility. *Ceram. Int.* **2016**, *42*, 466–480. [[CrossRef](#)]
15. Echavarría, A.M.; Rico, P.; Gómez Ribelles, J.L.; Pacha-Olivenza, M.A.; Fernández-Calderón, M.C.; Bejarano-G, G. Development of a Ta/TaN/TaN_x(Ag)_y/Ta_n nanocomposite coating system and bio-response study for biomedical applications. *Vacuum* **2017**, *145*, 55–67. [[CrossRef](#)]
16. Kuo, T.-Y.; Chin, W.-H.; Chien, C.-S.; Hsieh, Y.-H. Mechanical and biological properties of graded porous tantalum coatings deposited on titanium alloy implants by vacuum plasma spraying. *Surf. Coat. Technol.* **2019**, *372*, 399–409. [[CrossRef](#)]
17. Jin, W.; Wang, G.; Lin, Z.; Feng, H.; Li, W.; Peng, X.; Qasim, A.M.; Chu, P.K. Corrosion resistance and cytocompatibility of tantalum-surface-functionalized biomedical ZK60 Mg alloy. *Corros. Sci.* **2017**, *114*, 45–56. [[CrossRef](#)]
18. Balla, V.K.; Bodhak, S.; Bose, S.; Bandyopadhyay, A. Porous tantalum structures for bone implants: Fabrication, mechanical and in vitro biological properties. *Acta Biomater.* **2010**, *6*, 3349–3359. [[CrossRef](#)]
19. Hee, A.C.; Jamali, S.S.; Bendavid, A.; Martin, P.J.; Kong, C.; Zhao, Y. Corrosion behaviour and adhesion properties of sputtered tantalum coating on Ti6Al4V substrate. *Surf. Coat. Technol.* **2016**, *307*, 666–675. [[CrossRef](#)]
20. Cheng, Y.; Cai, W.; Li, H.T.; Zheng, Y.F.; Zhao, L.C. Surface characteristics and corrosion resistance properties of TiNi shape memory alloy coated with Ta. *Surf. Coat. Technol.* **2004**, *186*, 346–352. [[CrossRef](#)]
21. Yu, X.; Tan, L.; Yang, H.; Yang, K. Surface characterization and preparation of Ta coating on Ti6Al4V alloy. *J. Alloys Compd.* **2015**, *644*, 698–703. [[CrossRef](#)]
22. Alami, J.; Eklund, P.; Andersson, J.M.; Lattmann, M.; Wallin, E.; Bohlmark, J.; Persson, P.; Helmersson, U. Phase tailoring of Ta thin films by highly ionized pulsed magnetron sputtering. *Thin Solid Films* **2007**, *515*, 3434–3438. [[CrossRef](#)]
23. Myers, S.; Lin, J.; Souza, R.M.; Sproul, W.D.; Moore, J.J. The β to α phase transition of tantalum coatings deposited by modulated pulsed power magnetron sputtering. *Surf. Coat. Technol.* **2013**, *214*, 38–45. [[CrossRef](#)]
24. Maeng, S.; Axe, L.; Tyson, T.A.; Gladczuk, L.; Sosnowski, M. Corrosion behaviour of magnetron sputtered α - and β -Ta coatings on AISI 4340 steel as a function of coating thickness. *Corros. Sci.* **2006**, *48*, 2154–2171. [[CrossRef](#)]
25. Ebic, M.; Akar, S.; Akman, E.; Ozel, F.; Akin, S. The production and optimization of SnO₂ electron transporting layer by Slot-Die technique. *Int. J. Innov. Eng. Appl.* **2022**, *6*, 170–182.
26. Bilgic, A. Fabrication of monoBODIPY-functionalized Fe₃O₄@SiO₂@TiO₂ nanoparticles for the photocatalytic degradation of rhodamine B under UV irradiation and the detection and removal of Cu(II) ions in aqueous solutions. *J. Alloys Compd.* **2022**, *899*, 163360. [[CrossRef](#)]

27. Su, Y.; Huang, W.; Zhang, T.; Shi, C.; Hu, R.; Wang, Z.; Cai, L. Tribological properties and microstructure of monolayer and multilayer Ta coatings prepared by magnetron sputtering. *Vacuum* **2021**, *189*, 110250. [[CrossRef](#)]
28. Colin, J.J.; Abadias, G.; Michel, A.; Jaouen, C. On the origin of the metastable β -Ta phase stabilization in tantalum sputtered thin films. *Acta Mater.* **2017**, *126*, 481–493. [[CrossRef](#)]
29. Ji, P.; Liu, S.; Deng, H.; Ren, H.; Zhang, J.; Sun, T.; Xu, K.; Shi, C. Effect of magnetron-sputtered monolayer Ta and multilayer Ti-Zr-Ta and Zr-Ti-Ta coatings on the surface properties of biomedical Ti-6Al-4V alloy. *Mater. Lett.* **2022**, *322*, 132464. [[CrossRef](#)]
30. Sui, X.; Li, G.; Jiang, C.; Gao, Y.; Wang, K.; Wang, Q. Improved surface quality of layered architecture TiAlTaN/Ta coatings for high precision micromachining. *Surf. Coat. Technol.* **2017**, *320*, 298–303. [[CrossRef](#)]
31. Raszewski, Z. Evaluation of cytotoxic properties of some dental materials. *Appl. Biol. Res.* **2021**, *23*, 293–297.
32. Kokubo, T.; Takadama, H. How useful is SBF in predicting in vivo bone bioactivity? *Biomaterials* **2006**, *27*, 2907–2915. [[CrossRef](#)] [[PubMed](#)]
33. Simpson, R.; White, R.G.; Watts, J.F.; Baker, M.A. XPS investigation of monatomic and cluster argon ion sputtering of tantalum pentoxide. *Appl. Surf. Sci.* **2017**, *405*, 79–87. [[CrossRef](#)]
34. Abd El-Rahman, A.M.; Wei, R. Effect of ion bombardment on structural, mechanical, erosion and corrosion properties of Ti-Si-C-N nanocomposite coatings. *Surf. Coat. Technol.* **2014**, *258*, 320–328. [[CrossRef](#)]
35. Leyland, A.; Matthews, A. On the significance of the H/E ratio in wear control: A nanocomposite coating approach to optimised tribological behaviour. *Wear* **2000**, *246*, 1–11. [[CrossRef](#)]
36. Yue, Y.; Liu, S.; Qiu, W.; Wang, F.; Xue, Y.; Xia, C.; Du, S. Comparative Study on Wear Behaviors of Monolayer and Hetero-geneous Multilayer Ta Coatings in Atmospheric and SBF Environments. *Coatings* **2023**, *13*, 120. [[CrossRef](#)]
37. Li, Y.; Wong, C.; Xiong, J.; Hodgson, P.; Wen, C. Cytotoxicity of Titanium and Titanium Alloying Elements. *J. Dent. Res.* **2010**, *89*, 493–497. [[CrossRef](#)] [[PubMed](#)]
38. Metikoš-Huković, M.; Kwokal, A.; Piljac, J. The influence of niobium and vanadium on passivity of titanium-based implants in physiological solution. *Biomaterials* **2003**, *24*, 3765–3775. [[CrossRef](#)]

Disclaimer/Publisher's Note: The statements, opinions and data contained in all publications are solely those of the individual author(s) and contributor(s) and not of MDPI and/or the editor(s). MDPI and/or the editor(s) disclaim responsibility for any injury to people or property resulting from any ideas, methods, instructions or products referred to in the content.